RESEARCH ARTICLE

Performance Analysis of Downlink Polarized Distributed Antenna Systems With Antenna Selection Diversity

JUNGSUN UM[1] AND JAEHYUN PARK[2], (Member, IEEE)

[1]Media Broadcasting Research Section, Electronics and Telecommunications Research Institute, Daejeon 34129, South Korea
[2]School of Electronics and Communications Engineering, Pukyong National University, Busan 48513, South Korea

Corresponding author: Jaehyun Park (jaehyun@pknu.ac.kr)

ABSTRACT In this paper, we consider a distributed antenna system (DAS) with polarized antennas for the industrial internet-of-things, where distributed sensor nodes (SNs) with a single antenna are served by the closest distributed antenna (DA) port having multiple antennas. By using stochastic geometry, the interference in the polarized DAS is analyzed and the channel outage probability (OP) of the polarized DAS is also derived in a closed form. From the analytic results, the optimal vertically/horizontally polarized node densities are derived to minimize the channel OP. Furthermore, by investigating the effects of node density and polarization on the channel OP, we also develop a dual-polarized DAS, in which the effective density of co-polarized DA ports is the same with the density of all DA ports and, simultaneously, the interference from the active cross-polarized DA ports is effectively mitigated. By analyzing the channel OP for the dual-polarized DAS, the optimal node densities to minimize the overall channel OP and the effect of network design parameters on the channel OP is also investigated, which gives us a useful insight into the design of the polarized DAS.

INDEX TERMS Polarized distributed antenna system, stochastic geometry, industrial Internet of Things (IIoT).

I. INTRODUCTION

The industrial internet of things (IIoT) is envisioned to establish flexible and reconfigurable production systems in the manufacturing industry, because it connects massive devices and enables their autonomous data exchange [1], [2] and references therein. To support the reliable connectivity of massive sensor nodes (SNs), a distributed antenna system (DAS) has been extensively investigated [3], [4], [5], because it can take advantages of uniform service coverage with smaller path-loss, compared to the colocated antenna system. In [4], wireless power transfer architecture based on DAS is proposed and in [5], QoS-aware distributed antenna selection

The associate editor coordinating the review of this manuscript and approving it for publication was Mohamed M. A. Moustafa.

scheme is developed. Various beamforming techniques are also extensively investigated in DAS framework [6], [7]. However, these multi-antenna based transmission schemes assume the perfect channel state information (CSI) at transmitter, which causes time delay unsuitable for IIoT applications. Accordingly, transmit antenna selection schemes are investigated to maximize the achievable sum-rate [8] and minimize the power consumption [9] in DAS.

To lesson the spatial interference in communication networks, the antenna polarization can be used. In [10], dual-structured linear precoding scheme is proposed when the base station and the mobile stations are equipped with multi-polarized antennas and imperfect CSIT is available. In [11], quaternion-valued multi-user MIMO equalization is studied for the case of dual-polarized antennas and

in [12], joint transmitter-receiver design for multi-user MIMO transmission aided by polarization multiplexing is developed. Furthermore, the dual-polarized antenna has been exploited in a variety of sensor networks. In [13], the dual-polarized MIMO antenna systems are investigated to obtain the polarization diversity in cognitive radio ultra-wide band sensor networks. In [14], the dual-polarized antenna is developed for medical body-area networks (MBAN) covering the MBAN band (2.38-2.45 GHz) and a 5.8 GHz ISM bands (5.725-5.875 GHz). In [15], the dual-polarized antenna array is developed for wireless data and power transfer in the spectrum band of 4.5-5.8 GHz. Recently, the distributed MIMO with dual-polarized antennas has been also considered for the 5G new radio (NR) standardization [16], in which each DA port exploits 32 antenna elements. Dual-polarized antennas with high cross-polarization discrimination (XPD) have been developed [17], [18] and because of this, transmission techniques utilizing the polarization are becoming more critical in the interference management in DAS.

Note that the uncoordinated interference from distributed antenna (DA) ports which are randomly deployed in a given area degrades the system performance of DAS. Accordingly, the stochastic interference has been extensively investigated in DAS by exploiting the stochastic geometry [19], [20], [21] and references therein. That is, because the uncoordinated interference limits the system performance, to reduce the interference at the reference SN, multi-antenna-based techniques and DA cooperation schemes are proposed and their performances are analytically analyzed. In [19], the downlink spectral efficiency of multi-cell multi-user DAS is analyzed by using stochastic geometry when the maximal ratio transmission (MRT) and zero-forcing (ZF) beamforming is exploited at each DA port and perfect CSI is known at each DA port. In [20], when DA ports and sensor nodes have a single antenna, the spectral efficiency formulas for the blanket and selective transmission schemes are derived by exploiting stochastic geometry. In [21], a unified approach to analyze error probability, channel outage probability (OP), and transmission rate analysis in DAS by exploiting stochastic geometry is presented. In addition, we also note that the assumption of homogeneous Poisson point process (PPP) has been utilized to analyze the system performance for many different types of randomly distributed communication nodes. To see its validity, in [22], the deployment of the actual LTE base-stations (BSs) are compared to a sample of BSs from the PPP of the same BS density. Furthermore, the assumption of homogeneous PPP gives us a tight lower bound of the system performance compared to that with actual LTE BS deployment. Accordingly, the homogenous PPP has been widely used to model a variety of networks – cellular networks [23], [24], mobile ad hoc networks [25], [26], cognitive radio networks [27] and wireless sensor network [28], [29], [30]. However, the stochastic interference due to the polarized antennas in DAS has not been analyzed and its effect on the channel outage has not been investigated.

In this paper, we consider the downlink DAS with polarized antennas for IIoT,[1] where distributed SNs with a single antenna are served by the closest DA port having multiple antennas and the polarized antennas are exploited to mitigate the spatial interference. We assume that the serving DA port do not have full CSIT and transmit antenna selection diversity scheme is utilized because it requires less feedback overhead. We note that the antenna selection is expected to improve system performance while reducing the hardware complexity (i.e., reducing the number of RF chain) as well as the feedback overhead (the feedback latency and the feedback bits) [35], [36]. Likewise, because the smart factory applications require low-latency and the SN are resource limited in general, we consider the antenna selection scheme. By using stochastic geometry, the interference in the polarized DAS is first analyzed. Specifically, when each DA port has either vertically or horizontally polarized multiple antennas and each SN has a single polarized antenna, Laplace transform of the interference is derived and the channel OP of the polarized DAS is then derived in a closed form. Due to the tractability of PPP described in [23], [28], [29], and [30], we also assume that the nodes forms a PPP. From the analytic results, we show how we can optimize network parameters to minimize the channel OP. Specifically, the optimal vertically/horizontally polarized node densities for the polarized DAS are derived. Furthermore, by investigating the effects of node density and polarization on the channel OP, we also develop a dual-polarized DAS in which the DA port density is maintained compared to the conventional DAS, while the interference can be lessened through the polarization selection. In Table 1, we summarize and compare the relevant papers for the convenience of readers and, considering the polarized DAS, the contributions of this paper are listed below:

- Considering the single-polarized downlink DAS, assuming that SNs having a single antenna with either vertical or horizontal polarization are randomly distributed according to independent homogeneous PPP,[2] we investigate the channel OP by using the stochastic geometry. When each SN is served by a single co-polarized DA port having the minimum distance (equivalently, the minimum path-loss), the channel OP can be derived

---

[1] As specific applications, smart factories [32] and advanced cellular networks [16], [33], [34] with high node densities are considered, where the devices and the industrial equipment in a factory environment are wirelessly connected and the industrial processes are managed and controlled remotely. The interference analysis and the DAS design strategies developed in this paper can be extended to other applications with distributed sensor networks.

[2] Throughout the paper, we do not consider the exclusion zones around nodes that need to be protected from excessive interference generated by the cross-polarized DA ports, because the interference from the cross-polarized DA ports are naturally attenuated due to the XPD. However, if the exclusion zones are introduced through appropriate MAC protocols, the polarized DAS can be modeled as Poisson hole process (PHP), which is also used to describe the two-tier heterogeneous networks, and the PHP is also approximated as a homogeneous PPP through the first-order statistic approximation method [26]. Accordingly, the polarization density would be further optimized with the exclusion zone to manage the spatial interference, which is an interesting topic, but we believe it is out of scope of this paper.

TABLE 1. Literature review related to polarized DAS.

Ref.	Stochastic interference analysis	Consideration of polarized antennas	Multiple antennas at DA ports	Optimization of polarized node densities	CSIT (Type of CSI feedback)
[19]	✓	✗	✓	✗	Perfect CSIT (Full CSI)
[20]	✓	✗	✗	✗	No CSIT (N/A)
[28], [29]	✓	✗	✗	✗	No CSIT (N/A)
[30]	✓	✗	✓	✗	Perfect CSIT (Full CSI)
[31]	✓	✗	✓	✗	Perfect/Partial CSIT (Full CSI/Transmit antenna index)
[6], [7]	✗	✗	✓	✗	Perfect CSIT (Full CSI)
[8], [9]	✗	✗	✓	✗	Partial CSIT (Transmit antenna index)
[11], [12]	✗	✓	✓	✗	Perfect CSIT (Full CSI)
[10]	✗	✓	✓	✗	Partial CSIT (Long-term CSI/ Dimension-reduced short-term CSI)
This work	✓	✓	✓	✓	Partial CSIT (Transmit antenna index)

in terms of the Laplace transform of interference in a given area, which depends on the active co-polarized/cross-polarized DA port densities as well as the XPD. In the prior works [28], [29], [30], [31], the stochastic interference due to the polarized antennas in DAS and its effect on the channel outage has not been investigated. For notational convenience, the DAS without consideration of the polarized antennas is referred as the conventional co-polarized DAS.

- By formulating the channel OP min-max problem, the optimal vertically/horizontally polarized node densities for single-polarized DAS are derived such that the maximum of the channel OP at the typical polarized SN is minimized. From the analytic results, it can be found that the interference level can be effectively lessened by exploiting the polarized antennas at the nodes. We note that, in the prior works [6], [7], [8], [9], [11], [12], the beamforming/precoding schemes are developed for the polarized DAS, but the stochastic interference due to the antenna polarization in DAS is not analytically investigated. Differently from the prior works, we show how to optimize the polarized node densities from the analytic channel OP derived through the stochastic geometry.

- Motivated from the analysis of channel OP in the single-polarized DAS, we develop a dual-polarized downlink DAS, in which each DA port has both vertically/horizontally polarized antennas and accordingly the effective density of the co-polarized DA ports is the same with the density of all DA ports. At the same time, the interference from the active cross-polarized DA ports is effectively reduced. The optimal node densities to minimize the overall channel OP is theoretically derived and the effect of the network design parameters (e.g., the number of transmit antennas, node densities, and XPDs) on the channel OP is investigated, which gives us a useful insight into the design of the polarized DAS. Specifically, when XPD is small or the number of Tx antennas become large, the dual-polarized DAS outperforms the conventional co-polarized DAS. Therefore, based on the network parameters such as the

number of transmit antennas and the XPDs, it can be chosen which DAS structure is suitable to minimize the channel OPs.

The rest of this paper is organized as follows. In Section II, we introduce the polarized DAS system model. In Section III, we derive the channel OP analytically and obtain the optimal polarized node densities for single-polarized DAS from those analytic results. In Section IV, we propose the dual-polarized DAS and discuss DAS design strategies for the polarized DAS. In Section V, we provide several simulation results and in Section VI we give our conclusion.

II. SYSTEM MODEL FOR A SINGLE-POLARIZED DAS

In Fig. 1, we consider the downlink single-polarized DAS, where DA ports have N single polarized transmit antennas and SNs have a single receive antenna. Specifically, each DA port has N either vertically or horizontally polarized antennas and each SN has a single antenna with either vertically or horizontally polarization. It is assumed that the SNs with a vertically (respectively, horizontally) polarized antenna are distributed according to independent homogeneous PPP $\Phi_{VS}(\lambda_{VS})$ with a density λ_{VS} (respectively, $\Phi_{HS}(\lambda_{HS})$ with a density λ_{HS}). In addition, DA ports with vertically (respectively, horizontally) polarized antennas are assumed to be distributed according to independent homogeneous PPP $\Phi_{VD}(\lambda_{VD})$ with a density λ_{VD} (respectively, $\Phi_{HD}(\lambda_{HD})$ with a density λ_{HD}). If each DA port serves the closest co-polarized SN, active DA ports with vertically and horizontally polarization can be approximated by independent homogeneous PPPs $\Phi(\lambda_{AVD})$ and $\Phi(\lambda_{AHD})$, respectively [20], [37]. Here, the active node density can be given as $\lambda_{AVD} \approx \lambda_{VS}$ and $\lambda_{AHD} \approx \lambda_{HS}$.

Thanks to the Slivnyak's theorem [38], we analyze the network performance, conditioning on the existence of a "typical reference SN with either vertically or horizontally polarized antenna" at the origin. Without loss of generality, we can have $\Phi_D(\lambda_{pS}) = \{(r_{pi}, \mathbf{h}_{pi}), i = 0, 1, 2, \ldots\}$, where r_{pi} is the ascending ordered distances of the DA ports from the origin (i.e., $r_{pi} < r_{pi+1}$) with the antenna polarization $p \in \{V, H\}$. In addition, $\mathbf{h}_{pi} \sim \mathcal{CN}(0, \mathbf{I}_N)$, $p \in \{V, H\}$ denote short-term fading vector from the ith active DA port with
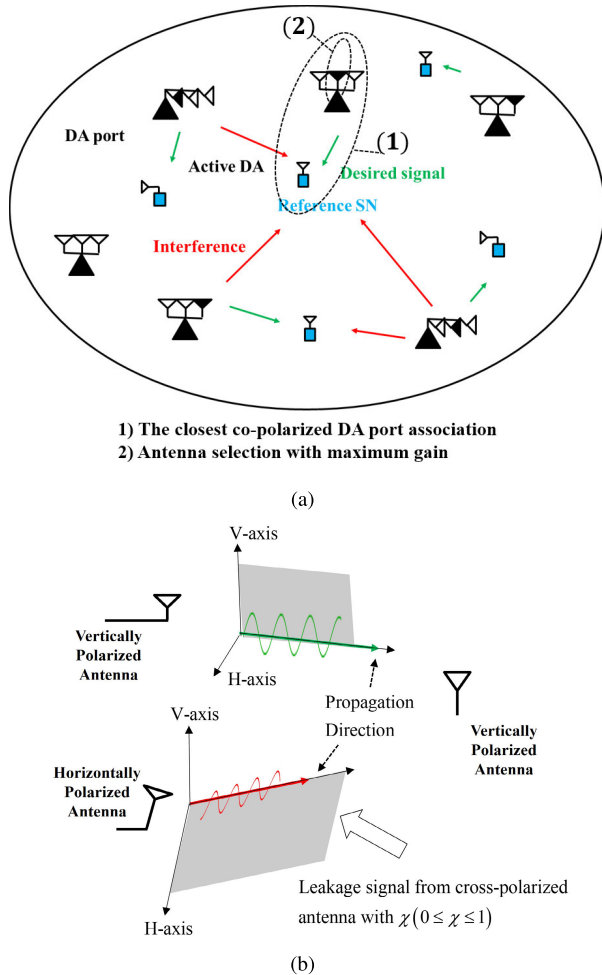
FIGURE 1. (a) The operation of downlink single-polarized DAS and (b) the signal propagation patterns emitted from vertically/horizontally polarized antennas.

the antenna polarization p to the reference SN. Because the reference SN is served by the DA port with the same polarized antennas and the minimum distance r_{p0}, $p \in \{V, H\}$, the received signal at the reference SN is then given as

$$y_{p0} = r_{p0}^{-\alpha/2}\mathbf{h}_{p0}^H\mathbf{x}_{p0} + \sum_{i \in \Phi(\lambda_{pS})/r_{p0}} r_{pi}^{-\alpha/2}\mathbf{h}_{pi}^H\mathbf{x}_{Vi}$$
$$+ \sqrt{\chi}\sum_{i \in \Phi(\lambda_{\tilde{p}S})} r_{\tilde{p}i}^{-\alpha/2}\mathbf{h}_{\tilde{p}i}^H\mathbf{x}_{\tilde{p}i} + n_0, \quad (1)$$

where $\mathbf{x}_{pi}$ denotes a transmit signal vector from the ith DA port with the polarization p and $\tilde{p} = \begin{cases} H & \text{if } p = V \\ V & \text{if } p = H \end{cases}$. In addition, n_0 denotes a zero-mean additive white Gaussian noise with a variance σ_n^2, and α is a path-loss exponent. The parameter $0 \leq \chi \leq 1$ is the inverse of the XPD, $1 \leq$ XPD $\leq \infty$ (See also Fig. 1(b).). Here, XPD refers to the long-term statistics of antenna elements and channel depolarization that measures the ability to distinguish the orthogonal polarization. The distance r_{p0} is a RV with the probability density function (PDF) given as [23]

$$f_{r_{p0}}(r) = 2\pi\lambda_{pD}re^{-\pi\lambda_{pD}r^2}, r > 0. \quad (2)$$

Throughout the paper, we assume that instantaneous full CSIT is not available because the feedback channel is hardly implemented or transfers one or few bits due to the requirement of low-latency in IIoT. Accordingly, long-term CSIT (e.g., the path-loss exponent and the XPD) is available at the DA ports and the antenna index (requiring few bits) can be fed back from SNs. Therefore, in this paper, the transmit antenna selection scheme is considered. That is, $\mathbf{x}_{pi}$, $p \in \{V, H\}$ are given as $\mathbf{x}_{pi} = \mathbf{w}_i s_{pi}$, where s_{pi} is the data symbol stream for the ith SN with p-polarized antenna and $E[|s_{pi}|^2] = P_{tx}$, and $\mathbf{w}_i$ is the antenna selection vector, given as $\mathbf{w}_i = [0, \ldots, 0, 1, 0, \ldots, 0]^T (\in \mathbb{R}^{N \times 1})$ such that only one antenna element with the maximum channel gain in $\mathbf{h}_{pi}$ is selected.

In addition, the SINR at the reference SN with the polarization p, γ_{p0}, is given as

$$\gamma_{p0} = \frac{r_{p0}^{-\alpha}|h_{p\,\max}|^2}{IN_{p0}}, \quad (3)$$

where $h_{p\,\max} = \max_{i=1,\ldots,N}|[\mathbf{h}_{p0}]_i|$ and

$$IN_{p0} = I_{\Phi(\lambda_{pp})}|r_{p0} + I_{\Phi(\lambda_{p\tilde{p}})} + \sigma_n^2/P_{tx} \quad (4)$$

with $I_{\Phi(\lambda_{pp})}|r_{p0} = \sum_{i \in \Phi(\lambda_{pS})/r_{p0}} r_{pi}^{-\alpha}|[\mathbf{h}_{pi}]_{k_i}|^2$ and $I_{\Phi(\lambda_{p\tilde{p}})} = \chi\sum_{i \in \Phi(\lambda_{\tilde{p}S})} r_{\tilde{p}i}^{-\alpha}|[\mathbf{h}_{\tilde{p}i}]_{k_i}|^2$. Here k_i is the antenna index selected at the ith SN.

III. ANALYSIS OF CHANNEL OUTAGE PROBABILITY FOR THE SINGLE-POLARIZED DAS
A. DERIVATION OF CHANNEL OUTAGE PROBABILITY
Note that the squared norm of each element in $\mathbf{h}_{pi}$ for $p \in \{V, H\}$ and $i = 1, 2, \ldots$ is distributed according to the chi-squared distribution with a degree-of-freedom (DoF) of two. Accordingly, by defining $\Psi_0 \triangleq |h_{p\,\max}|^2$ and exploiting the order statistics [39], the complementary cumulative distribution function (CCDF) of Ψ_0, denoted as $F_{\Psi_0}^c(x)$, can be derived as

$$F_{\Psi_0}^c(x) = P(\Psi_0 > x) = 1 - (1 - e^{-x})^N$$
$$= \sum_{n=1}^N {}_NC_n(-1)^{n+1}e^{-nx}, \quad (5)$$

where ${}_NC_n = \frac{N!}{n!(N-n)!}$. We also define $\Psi_{pi} \triangleq |[\mathbf{h}_{pi}]_{k_i}|^2$ and $\Psi_{\tilde{p}i} \triangleq |[\mathbf{h}_{\tilde{p}i}]_{k_i}|^2$. Then, they follows the chi-squared distribution with a DoF of two, which are denoted as

$$\Psi_{pi} \sim \chi_2^2, \qquad \Psi_{\tilde{p}i} \sim \chi_2^2, \quad i = 1, 2, \ldots \quad (6)$$

From [31], by exploiting the CCDF of Ψ_0, $P(\gamma_0 \geq \bar{\gamma}_{th})$ for a given $r_{p0} = r$ can be derived as

$$P(\gamma_0 \geq \bar{\gamma}_{th}|r_{p0} = r) = P\left(|h_{p\,\max}|^2 \geq \bar{\gamma}_{th}IN_{p0}r^\alpha\right)$$
$$= \int_0^\infty P\left(|h_{p\,\max}|^2 \geq s\bar{\gamma}_{th}r^\alpha\right)f_{IN_{p0}}(s)ds$$
$$= \int_0^\infty F_{\Psi_0}^c(s\bar{\gamma}_{th}r^\alpha)f_{IN_{p0}}(s)ds, \quad (7)$$

where $f_{IN_{p0}}(s)$ is the PDF of IN_{p0} in (4). Therefore, from (2), (5) and (7), the channel outage probability can be derived as

$$P(\gamma_0 < \bar{\gamma}_{th}) = 1 - \int_0^\infty \left(2\pi \lambda_{pD} r e^{-\pi \lambda_{pD} r^2} \sum_{n=1}^N {}_N C_n (-1)^{n+1} \right.$$
$$\left. \times L_{IN_{p0}|r}(z) \big|_{z=n\bar{\gamma}_{th} r^\alpha} \right) dr. \quad (8)$$

In (8), $L_{IN_{p0}|r}(z)$ is the Laplace transform of the interference and noise power from active DA ports affecting a receiver located r meters away from its serving DA port. Here, for high SNR regime, it can be given as

$$L_{IN_{p0}|r}(z) \approx L_{I_{\Phi(\lambda_{pS})}|r}(z) L_{I_{\Phi(\lambda_{\tilde{p}S})}|r}(z), \quad (9)$$

where the first term is associated with the interference from co-polarized DA ports and the second term is due to the interference from cross-polarized DA ports. From [21] and [31], $L_{I_{\Phi(\lambda_{pS})}|r}(z)$ and $L_{I_{\Phi(\lambda_{\tilde{p}S})}|r}(z)$ in (9) are respectively derived as

$$L_{I_{\Phi(\lambda_{pS})}|r}(z)$$
$$= E\left[\exp\left[-z \sum_{i \in \Phi(\lambda_{pS})/r} r_i^{-\alpha} \Psi_{pi} \right] \right]$$
$$= \exp\left[-2\pi \lambda_{pS} \int_r^\infty E_{\Psi_{pi}} \left[1 - \exp[-z r^{-\alpha} \Psi_{pi}] \right] r dr \right]$$
$$= \exp\left[-2\pi \lambda_{pS} \int_r^\infty \left[1 - \frac{1}{(1+z r^{-\alpha})} \right] r dr \right], \quad (10)$$

and

$$L_{I_{\Phi(\lambda_{\tilde{p}S})}|r}(z)$$
$$= E\left[\exp\left[-z\chi \sum_{i \in \Phi(\lambda_{\tilde{p}S})/r} r_i^{-\alpha} \Psi_{\tilde{p}i} \right] \right]$$
$$= \exp\left[-2\pi \lambda_{\tilde{p}S} \int_0^\infty E_{\Psi_{\tilde{p}i}} \left[1 - \exp[-z\chi r^{-\alpha} \Psi_{\tilde{p}i}] \right] r dr \right]$$
$$= \exp\left[-2\pi \lambda_{\tilde{p}S} \int_0^\infty \left[1 - \frac{1}{(1+z\chi r^{-\alpha})} \right] r dr \right]. \quad (11)$$

From Lemma 1 of [40], $L_{I_{\Phi(\lambda_{pS})}|r}(z)$ and $L_{I_{\Phi(\lambda_{\tilde{p}S})}|r}(z)$ can be further simplified below, which gives us a useful insight.

$$L_{I_{\Phi(\lambda_{pS})}|r}(z) = \exp\left[-\lambda_{pS} z^{\frac{2}{\alpha}} C_{co}(\alpha, z) \right], \quad (12)$$

$$L_{I_{\Phi(\lambda_{\tilde{p}S})}|r}(z) = \exp\left[-\lambda_{\tilde{p}S} \chi^{\frac{2}{\alpha}} z^{\frac{2}{\alpha}} C_{cr}(\alpha) \right], \quad (13)$$

where

$$C_{co}(\alpha, z) = \frac{2\pi}{\alpha} \left(B(\frac{2}{\alpha}, 1 - \frac{2}{\alpha}) - B(\frac{1}{1+z r^{-\alpha}}, \frac{2}{\alpha}, 1 - \frac{2}{\alpha}) \right),$$
$$C_{cr}(\alpha) = \frac{2\pi}{\alpha} B(\frac{2}{\alpha}, 1 - \frac{2}{\alpha}).$$

Here, $B(a, b)$ and $B(x; a, b)$ are beta/incomplete beta functions, respectively, given as $B(a, b) = \frac{\Gamma(a)\Gamma(b)}{\Gamma(a+b)}$ and $B(x; a, b) = \int_0^x u^{a-1}(1-u)^{b-1} du$. For compactness, the detailed derivation is omitted, but (12) and (13) can be

obtained from the change of variables in the integration in (10) and (11) as similar steps in Lemma 1 of [40]. We note that because the co-polarized DA port with the minimum distance r is selected, the co-polarized DA ports within a radius r from the typical SN do not cause interference, resulting that the integration starts from r in (10).

From the discussion above, the channel outage probability for the polarized DAS can be derived.

Theorem 1: When active DA ports with vertically and horizontally polarization are distributed according to independent homogeneous PPPs, $\Phi_{VS}(\lambda_{VS})$ with a density λ_{VS} and $\Phi_{HS}(\lambda_{HS})$ with a density λ_{HS}), the channel outage probability at the typical SN with p polarization, ($p \in \{V, H\}$, is given as the closed form as

$$P_{out,p}$$
$$= P(\gamma_0 < \bar{\gamma}_{th})$$
$$= 1 - \sum_{n=1}^N \frac{\pi \lambda_{pD} {}_N C_n (-1)^{n+1}}{\pi \lambda_{pD} + \left(\lambda_{pS} C_{co}(\alpha, n) + \chi^{\frac{2}{\alpha}} \lambda_{\tilde{p}S} C_{cr}(\alpha) \right) (n\bar{\gamma}_{th})^{\frac{2}{\alpha}}}$$
$$\quad (14)$$

where

$$C_{co}(\alpha, n) = C_{co}(\alpha, z) \big|_{z=n\bar{\gamma}_{th} r^\alpha}$$
$$= \frac{2\pi}{\alpha} \left(B(\frac{2}{\alpha}, 1 - \frac{2}{\alpha}) - B(\frac{1}{1+n\bar{\gamma}_{th}}, \frac{2}{\alpha}, 1 - \frac{2}{\alpha}) \right)$$
$$= \frac{2\pi}{\alpha} B\left(\frac{n\bar{\gamma}_{th}}{1+n\bar{\gamma}_{th}}, \frac{2}{\alpha}, 1 - \frac{2}{\alpha} \right), \quad (15)$$

Proof: From (9), (12), and (13), for the typical SN with vertical polarization, the Laplace transform, $L_{IN_{p0}|r}(z)$, at $z = n\bar{\gamma}_{th} r^\alpha$ can be approximated as

$$L_{IN_{p0}|r}(z) \big|_{z=n\bar{\gamma}_{th} r^\alpha}$$
$$\approx L_{I_{\Phi(\lambda_{pS})}|r}(z) L_{I_{\Phi(\lambda_{\tilde{p}S})}|r}(z) \big|_{z=n\bar{\gamma}_{th} r^\alpha}$$
$$= \exp\left[-\left(\lambda_{pS} C_{co}(\alpha, n) + \chi^{\frac{2}{\alpha}} \lambda_{\tilde{p}S} C_{cr}(\alpha) \right) (n\bar{\gamma}_{th})^{\frac{2}{\alpha}} r^2 \right]. \quad (16)$$

Accordingly, (8) can be rewritten as (17), shown at the bottom of the next page, and after simple algebraic manipulations, (14) can be derived.

□

We note that, because the feedback overhead to obtain the perfect CSIT is prohibitive in IIoT due to the requirement of low-latency in IIoT, the transmit antenna selection scheme is considered. However, if the perfect CSIT is available, the maximal ratio transmission scheme can be employed at each DA port, resulting in more SINR improvement at the SN. Specifically, the CCDF of Ψ_0 in (5) will be given as a similar form derived in [31] and the proposed analysis and design strategies can be incorporated with and extended to the perfect/more strong CSIT scenarios, and a more detailed investigation is left as our future work.

To see how the outage probability in (14) is relevant to the hardware specification, let us consider that the transmission

bandwidth and the packet duration are, respectively, given by BW and T_p. For the packet size of N_b bits, the outage probability can be given as

$$
\begin{aligned}
P_{out} &= P\left(BW \log_2(1 + \gamma_0) < \frac{N_b}{T_p} \right) \\
&= P\left(\gamma_0 < 2^{\frac{N_b}{BWT_p}} - 1 \right).
\end{aligned} \tag{18}
$$

Therefore, the outage probability depends on the transmission bandwidth, the packet duration, and the packet size and $\bar{\gamma}_{th}$ in (14) can be expressed as $\bar{\gamma}_{th} = 2^{\frac{N_b}{BWT_p}} - 1$.

B. OPTIMAL VERTICALLY/HORIZONTALLY POLARIZED NODE DENSITIES FOR THE SINGLE-POLARIZED DAS

Because both $P_{out,V}$ and $P_{out,H}$ in (14) should be minimized simultaneously, the optimization of node densities can be formulated as the following min-max problem:

$$
\begin{aligned}
(\hat{\lambda}_{VS}, &\hat{\lambda}_{HS}, \hat{\lambda}_{VD}, \hat{\lambda}_{HD}) \\
&= \underset{\substack{(\lambda_{VS}, \lambda_{HS}, \\ \lambda_{VD}, \lambda_{HD})}}{\arg\ \min} \max(P_{out,V}, P_{out,H}) \\
&\text{s.t. } \lambda_{VS} + \lambda_{HS} = \lambda_S, \quad \lambda_{pS} > 0 \\
&\qquad\ \ \lambda_{VD} + \lambda_{HD} = \lambda_D, \quad \lambda_{pD} > 0.
\end{aligned} \tag{19}
$$

The following lemma gives an insight into how to optimize the SN densities to minimize the channel outage probability.

Lemma 1: The following function, $f(x)$, is an increasing function with respect to x for a small $x > 0$.

$$
f(x) = 1 - \sum_{n=1}^{N} \frac{{}_N C_n (-1)^{n+1}}{1 + xn^{\frac{2}{\alpha}}}.
$$

Proof: Due to the limit of space, we omit the proof. □

We note that the channel outage in (14) can be given as

$$
P_{out,p} = 1 - \sum_{n=1}^{N} \frac{{}_N C_n (-1)^{n+1}}{1 + x_p n^{\frac{2}{\alpha}}},
$$

where $x_p = \dfrac{\left(\lambda_{pS} C_{co}(\alpha,n) + \chi^{\frac{2}{\alpha}} \lambda_{\bar{p}S} C_{cr}(\alpha) \right) \bar{\gamma}_{th}^{\frac{2}{\alpha}}}{\pi \lambda_{pD}}$ and x_p is usually small for $\lambda_{pD} > \lambda_S$ and small $\bar{\gamma}_{th}$. Therefore, from Lemma 1, to decrease the channel outage probability, x_p should be minimized and (38) can be rewritten as

$$
\begin{aligned}
(\hat{\lambda}_{VS}, \hat{\lambda}_{VD}) &= \underset{\lambda_{VS}, \lambda_{VD}}{\arg\ \min} \max (C_V, C_H) \\
&\text{s.t. } 0 < \lambda_{VS} < \lambda_S, \quad 0 < \lambda_{VD} < \lambda_D, \tag{20}
\end{aligned}
$$

where

$$
\begin{aligned}
C_V &= \frac{\lambda_{VS} C_{co}(\alpha,n) + \chi^{\frac{2}{\alpha}}(\lambda_S - \lambda_{VS}) C_{cr}(\alpha)}{\lambda_{VD}}, \\
C_H &= \frac{(\lambda_S - \lambda_{VS}) C_{co}(\alpha,n) + \chi^{\frac{2}{\alpha}} \lambda_{VS} C_{cr}(\alpha)}{\lambda_D - \lambda_{VD}}. \tag{21}
\end{aligned}
$$

and it can be found that, for the optimal $(\hat{\lambda}_{VS}, \hat{\lambda}_{VD})$,

$$
\begin{aligned}
&\frac{\hat{\lambda}_{VS} C_{co}(\alpha,n) + \chi^{\frac{2}{\alpha}}(\lambda_S - \hat{\lambda}_{VS}) C_{cr}(\alpha)}{\hat{\lambda}_{VD}} (= \hat{C}_V) \\
&= \frac{(\lambda_S - \hat{\lambda}_{VS}) C_{co}(\alpha,n) + \chi^{\frac{2}{\alpha}} \hat{\lambda}_{VS} C_{cr}(\alpha)}{\lambda_D - \hat{\lambda}_{VD}} (= \hat{C}_H). \tag{22}
\end{aligned}
$$

Otherwise, we can always find a new parameter set, $(\hat{\lambda}'_{VS}, \hat{\lambda}'_{VD})$, exhibiting smaller $C_{opt} < \min \max \left(\hat{C}_V, \hat{C}_H \right)$. We note that (22) can be rewritten as

$$
\frac{\hat{\lambda}_{HD}}{\hat{\lambda}_{VD}} = \frac{\hat{\lambda}_{HS} C_{co}(\alpha,n) + \chi^{\frac{2}{\alpha}} \hat{\lambda}_{VS} C_{cr}(\alpha)}{\hat{\lambda}_{VS} C_{co}(\alpha,n) + \chi^{\frac{2}{\alpha}} \hat{\lambda}_{HS} C_{cr}(\alpha)}. \tag{23}
$$

Accordingly, when the densities of polarized SNs are given, the portion of polarized DA ports can be determined from (23). For example, if λ_{VS} and λ_{HS} are given fixed and χ is small (i.e., (23) yields $\frac{\hat{\lambda}_{HD}}{\hat{\lambda}_{VD}} \approx \frac{\hat{\lambda}_{HS}}{\hat{\lambda}_{VS}}$.), it can be found that the p-polarized DA port density $\hat{\lambda}_{pD}$ is proportional to $\hat{\lambda}_{pS}$. When λ_{VS} and λ_{HS} are not given as fixed values, due to the symmetry of node densities in C_V and C_H, it can be found that $\hat{\lambda}_{VS} = \hat{\lambda}_{HS} = \frac{\lambda_S}{2}$ and therefore, $\hat{\lambda}_{VD} = \hat{\lambda}_{HD} = \frac{\lambda_D}{2}$.

Remark 1: From Theorem 1 and the above discussion, when the node densities are given as $\hat{\lambda}_{VS} = \hat{\lambda}_{HS} = \frac{\lambda_S}{2}$ and $\hat{\lambda}_{VD} = \hat{\lambda}_{HD} = \frac{\lambda_D}{2}$, the optimal outage probability for the single-polarized DAS can be given as

$$
\begin{aligned}
P_{out,SP} &= \min \max(P_{out,V}, P_{out,H}) \\
&= 1 - \sum_{n=1}^{N} \frac{{}_N C_n (-1)^{n+1}}{1 + \hat{x}_{SP} n^{\frac{2}{\alpha}}}, \tag{24}
\end{aligned}
$$

where

$$
\hat{x}_{SP} = \frac{\left(\lambda_S C_{co}(\alpha,n) + \chi^{\frac{2}{\alpha}} \lambda_S C_{cr}(\alpha) \right) \bar{\gamma}_{th}^{\frac{2}{\alpha}}}{\pi \lambda_D}. \tag{25}
$$

We note that by reducing the node density of co-polarized SNs, the interference from the active co-polarized DA ports can be reduced, and accordingly, the overall interference level can be reduced at the reference SN. However, half of DA ports have the co-polarized antennas with the reference SN

$$
\begin{aligned}
P(\gamma_0 < \bar{\gamma}_{th}) &= 1 - \sum_{n=1}^{N} {}_N C_n (-1)^{n+1} \int_0^{\infty} 2\pi \lambda_{pD} r \exp\left[-\left(\pi \lambda_{pD} + \left(\lambda_{pS} C_{co}(\alpha,n) + \chi^{\frac{2}{\alpha}} \lambda_{\bar{p}S} C_{cr}(\alpha) \right) (n\bar{\gamma}_{th})^{\frac{2}{\alpha}} \right) r^2 \right] dr \\
&= 1 - \sum_{n=1}^{N} {}_N C_n (-1)^{n+1} \frac{\pi \lambda_{pD}}{\pi \lambda_{pD} + \left(\lambda_{pS} C_{co}(\alpha,n) + \chi^{\frac{2}{\alpha}} \lambda_{\bar{p}S} C_{cr}(\alpha) \right) (n\bar{\gamma}_{th})^{\frac{2}{\alpha}}}
\end{aligned} \tag{17}
$$

and the others have cross-polarized antennas to support both polarized SNs in a given area and the reduced co-polarized DA port density increases the communication distance between the reference SN and its nearest co-polarized DA port from (2). Here, we note that, motivated from [41], the polarization can be actively selected at the node and therefore, the polarization density would be controllable with appropriate MAC protocols, which is an interesting topic, but we believe it is out of scope of this paper. □

Remark 2: By taking a similar approach in Theorem 1, the outage probability of the co-polarized DAS is derived as

$$P_{out,CP} = 1 - \sum_{n=1}^{N} \frac{{}_N C_n (-1)^{n+1}}{1 + \hat{x}_{CP} n^{\frac{2}{\alpha}}}, \quad (26)$$

where

$$\hat{x}_{CP} = \frac{(\lambda_S C_{co}(\alpha, n)) \bar{\gamma}_{th}^{\frac{2}{\alpha}}}{\pi \lambda_D}. \quad (27)$$

Here, we note that the conventional DAS, not considering the polarized antennas (i.e., DAS with co-polarized antennas) is regarded as the baseline system. In addition, the nodes have the same polarized antennas, which implies that there is no interference from the cross polarized DA ports. From (25) and (27), it can be found that $P_{out,CP} \leq P_{out,SP}$ and when $\chi = 0$, $P_{out,CP} = P_{out,SP}$. That is, the polarized DAS has the same channel outage performance with the conventional co-polarized DAS only when the polarized antenna nulls out the signal from the cross-polarized antennas perfectly. That is, the single-polarized DAS does not achieve the performance gain against the conventional co-polarized DAS. This is because the co-polarized DA port density is reduced as much as the overall interference level is lowered, which is also discussed in Remark 1. □

IV. DOWNLINK DAS WITH DUAL-POLARIZED ANTENNAS
Motivated from Remark 1 and 2, we develop the dual-polarized DAS, in which the effective density of the co-polarized DA ports is the same with the density of all DA ports (i.e., λ_D) and, simultaneously, the interference from the active cross-polarized DA ports is effectively reduced. That is, each DA port has vertically polarized antennas as well as horizontally polarized antennas and accordingly, SN can associate with the closest DA port regardless of the antenna polarization.
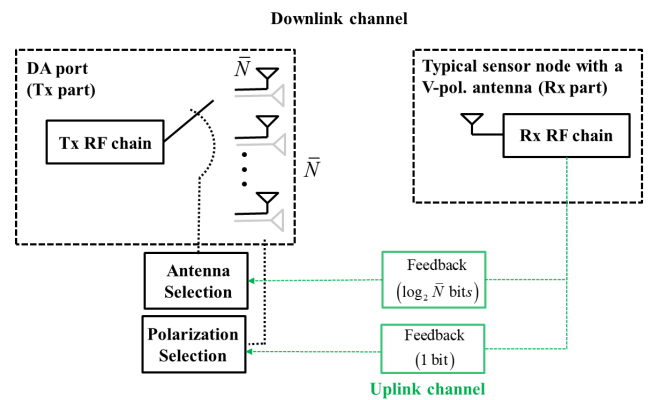
A. OPERATION OF DUAL-POLARIZED DAS
As in Fig. 2, by considering the dual-polarized DAS, if each DA port has $N/2$ vertically polarized antennas and $N/2$ horizontally polarized antennas and serves the closest SN by selecting its antenna polarization same with the associated SN, active DA ports with vertically and horizontally polarization can be approximated by independent homogeneous PPPs $\Phi(\lambda_{AVD})$ and $\Phi(\lambda_{AHD})$, respectively. Then, the serving DA port selects the co-polarized antenna with the maximum channel gain to transmit the desired signal
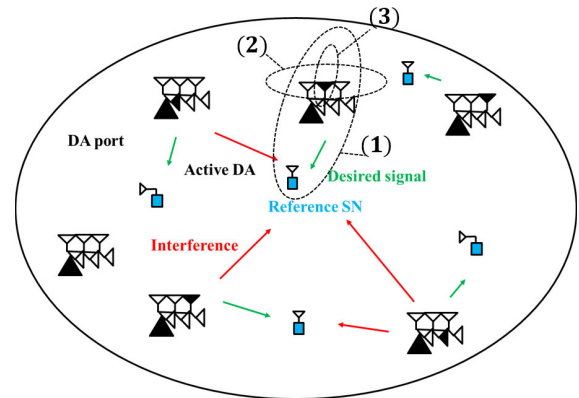
FIGURE 2. (a) The operation and (b) hardware configuration of downlink dual-polarized DAS.

to the reference SN. The received signal at the reference SN with p polarization is then given as

$$y_{p0} = r_0^{-\alpha/2} \mathbf{h}_{p0}^H \mathbf{x}_{p0} + \sum_{i \in \Phi(\lambda_{pS})/r_0} r_{pi}^{-\alpha/2} \mathbf{h}_{pi}^H \mathbf{x}_{pi}$$
$$+ \sqrt{\chi} \sum_{i \in \Phi(\lambda_{\tilde{p}S})/r_0} r_{\tilde{p}i}^{-\alpha/2} \mathbf{h}_{\tilde{p}i}^H \mathbf{x}_{\tilde{p}i} + n_0, \quad (28)$$

where $\mathbf{h}_{pi}, \mathbf{x}_{pi} \in \mathbb{C}^{\bar{N} \times 1}$ with $\bar{N} = N/2$ and the distance r_0 is a RV with the PDF given as

$$f_{r_0}(r) = 2\pi \lambda_D r e^{-\pi \lambda_D r^2}, r > 0. \quad (29)$$

Therefore, the SINR at the reference SNs with vertically/horizontally polarized antenna can be given as

$$\gamma_{p0} = \frac{r_0^{-\alpha} |h_{p\max}|^2}{I_{\Phi(\lambda_{pp})|r_0} + I_{\Phi(\lambda_{p\tilde{p}})|r_0} + \sigma_n^2/P_{tx}}, \quad (30)$$

where $p \in \{V, H\}$ and $\tilde{p} = \begin{cases} H \text{ if } p = V \\ V \text{ if } p = H \end{cases}$.

We note that the main differences between (1) and (28) are the PDF of the distance between the reference SN and its serving DA port and the number of co-polarized transmit

antennas at the serving DA port. That is, the minimum distance between the reference SN and its serving DA port in the dual-polarized DAS is smaller, while the number of co-polarized transmit antennas is a half of that in the single-polarized DAS. We also note that another big difference between the dual-polarized DAS and the conventional DAS, not considering the polarized antennas is the transmit antenna selection process. For the conventional DAS, after the closest DA port association, the sensor node reports the selected transmit antenna index back to the associated DA port through the feedback channel. Here, the feedback overhead is $\log_2 N$ bits for N transmit antennas.

For the dual-polarized DAS, after the closest DA port association, the polarization selection is processed at the associated DA port, requiring one bit feedback and then the sensor node reports the selected transmit antenna index back to the associated DA port. The associated antenna selection process is described in Fig. 2 (a), when the typical SN has a vertically polarized antenna. In addition, the detailed hardware configuration for the antenna selection process is described in Fig. 2 (b). A similar hardware configuration can be explained when the typical SN has a horizontally polarized antenna. Because, in the dual-polarized DAS, each DA port has $N/2$ vertically polarized antennas and $N/2$ horizontally polarized antennas, the required feedback overhead is $\log_2(N/2)$ bits for $N/2$ co-polarized transmit antennas. Therefore, the overall required feedback bits are the same for both systems. We also note that the antenna selection process developed in [42] and [43] can also be incorporated with our dual-polarized DAS.

B. OUTAGE PROBABILITY FOR DUAL-POLARIZED DAS

By taking a similar approach in the proof of Theorem 1, the channel outage probability for the dual-polarized DAS can also be derived as follows.

Theorem 2: For the dual-polarized DAS distributed according to homogeneous PPP $\Phi(\lambda_D)$ with a density λ_D, when SNs with vertically and horizontally polarization are distributed according to independent homogeneous PPPs, $\Phi_{VS}(\lambda_{VS})$ with a density λ_{VS} and $\Phi_{HS}(\lambda_{HS})$ with a density λ_{HS}), the channel outage probability at the typical SN with p polarization, ($p \in \{V, H\}$), is given as the closed form as

$$P_{out,p}$$
$$= P(\gamma_0 < \bar{\gamma}_{th})$$
$$= 1 - \sum_{n=1}^{\bar{N}} \frac{\pi \lambda_{D\bar{N}} C_n (-1)^{n+1}}{\pi \lambda_D + \left(\lambda_{pS} C_{co}(\alpha, n) + \chi^{\frac{2}{\alpha}} \lambda_{\tilde{p}S} C_{cr}(\alpha, n) \right) (n\bar{\gamma}_{th})^{\frac{2}{\alpha}}} \tag{31}$$

where $\tilde{p} = \begin{cases} H & \text{if } p = V \\ V & \text{if } p = H \end{cases}$ *and*

$$C_{co}(\alpha, n) = C_{co}(\alpha, z)|_{z=n\bar{\gamma}_{th}r^\alpha}$$
$$= \frac{2\pi}{\alpha} B\left(\frac{n\bar{\gamma}_{th}}{1 + n\bar{\gamma}_{th}}, \frac{2}{\alpha}, 1 - \frac{2}{\alpha} \right), \tag{32}$$

$$C_{cr}(\alpha, n) = C_{cr}(\alpha, z)|_{z=n\bar{\gamma}_{th}r^\alpha}$$
$$= \frac{2\pi}{\alpha} B\left(\frac{n\chi\bar{\gamma}_{th}}{1 + n\chi\bar{\gamma}_{th}}, \frac{2}{\alpha}, 1 - \frac{2}{\alpha} \right). \tag{33}$$

Corollary 1: When active DA ports with vertically and horizontally polarization are distributed according to independent homogeneous PPPs, $\Phi_{VS}(\lambda_{VS})$ with a density λ_{VS} and $\Phi_{HS}(\lambda_{HS})$ with a density λ_{HS}), the interference from the superposed PPPs ($\Phi(\lambda_{VS})$ and $\Phi(\lambda_{HS})$) with different polarization can be approximated as that from a homogeneous PPP with copolarized DAS and an effective node density ($\lambda_{VS} + \chi^{\frac{4}{\alpha}} \lambda_{HS}$) and the channel outage probability at the typical SN is given as the closed form as

$$P_{out,p} \approx 1 - \sum_{n=1}^{\bar{N}} \frac{\pi \lambda_{D\bar{N}} C_n (-1)^{n+1}}{\pi \lambda_D + \left(\lambda_{pS} + \chi^{\frac{4}{\alpha}} \lambda_{\tilde{p}S} \right) C_{co}(\alpha, n)(n\bar{\gamma}_{th})^{\frac{2}{\alpha}}}. \tag{34}$$

Proof: From the series formula for the incomplete Beta function [44], for small γ_{th}, $C_{co}(\alpha, n)$ in (32) can be approximated as

$$C_{co}(\alpha, n) \approx \frac{2\pi}{\alpha} B\left(n\bar{\gamma}_{th}, \frac{2}{\alpha}, 1 - \frac{2}{\alpha} \right)$$
$$= \frac{2\pi}{\alpha} \left(\frac{\alpha}{2} (n\bar{\gamma}_{th})^{\frac{2}{\alpha}} + O\left((n\bar{\gamma}_{th})^{1+\frac{2}{\alpha}} \right) \right). \tag{35}$$

Likewise, $C_{cr}(\alpha, n)$ in (33) can be approximated as

$$C_{cr}(\alpha, n) \approx \frac{2\pi}{\alpha} B\left(n\chi\bar{\gamma}_{th}, \frac{2}{\alpha}, 1 - \frac{2}{\alpha} \right)$$
$$= \frac{2\pi}{\alpha} \left(\frac{\alpha}{2} (n\chi\bar{\gamma}_{th})^{\frac{2}{\alpha}} + O\left((n\chi\bar{\gamma}_{th})^{1+\frac{2}{\alpha}} \right) \right). \tag{36}$$

Accordingly, for small γ_{th}, $C_{cr}(\alpha, n) \approx \chi^{\frac{2}{\alpha}} C_{co}(\alpha, n)$ and the Laplace transform, $L_{IN_0|r}(z)$ can be approximated as

$$L_{IN_0|r}(z) \approx \exp\left[-\left(\lambda_{pS} + \chi^{\frac{4}{\alpha}} \lambda_{\tilde{p}S} \right) z^{\frac{2}{\alpha}} C_{co}(\alpha, n) \right]. \tag{37}$$

By comparing it with (12), the interference from the cross-polarized DA ports can be regarded as the interference from the co-polarized DA ports with the reduced node density, $\chi^{\frac{4}{\alpha}} \lambda_{\tilde{p}S}$. Therefore, by taking a similar approach in Theorem 1, the channel OP can be derived as (34). ☐

C. OPTIMAL VERTICALLY/HORIZONTALLY POLARIZED SN DENSITIES FOR DUAL-POLARIZED DAS

We note that in the dual-polarized DAS with a given DA port density, λ_D, the densities of the DA ports, in which the p-polarized antenna is selected and active, are determined according to the p-polarized SN densities. In addition, because both $P_{out,V}$ and $P_{out,H}$ in (31) should be minimized simultaneously, the optimization of SN densities can then be formulated as the following min-max problem:

$$(\hat{\lambda}_{VS}, \hat{\lambda}_{HS}) = \underset{(\lambda_{VS}, \lambda_{HS})}{\arg \min} \max(P_{out,V}, P_{out,H})$$
$$\text{s.t. } \lambda_{VS} + \lambda_{HS} = \lambda_S. \tag{38}$$

We note that the channel outage in (31) can be given as

$$P_{out,p} = 1 - \sum_{n=1}^{\bar{N}} \frac{{}^{\bar{N}}C_n(-1)^{n+1}}{1 + x_p n^{\frac{2}{\alpha}}},$$

where $x_p = \frac{\left(\lambda_{pS} C_{co}(\alpha,n) + \chi^{\frac{2}{\alpha}} \lambda_{\tilde{p}S} C_{cr}(\alpha,n) \right) \bar{\gamma}_{th}^{\frac{2}{\alpha}}}{\pi \lambda_D}$ and x_p is usually small for $\lambda_D > \lambda_S$ and small $\bar{\gamma}_{th}$. Therefore, from Lemma 1, to decrease the channel OP, λ_D should be increased and simultaneously, $\left(\lambda_{pS} C_{co}(\alpha,n) + \chi^{\frac{2}{\alpha}} \lambda_{\tilde{p}S} C_{cr}(\alpha,n) \right)$ should be decreased. Accordingly, the optimization in (38) can be equivalently transformed into the optimization of λ_{VS} as

$$\hat{\lambda}_{VS}$$
$$= \arg\max_{\lambda_{VS}} \min \left(\left(\lambda_{VS} C_{co}(\alpha,n) + \chi^{\frac{2}{\alpha}} (\lambda_S - \lambda_{VS}) C_{cr}(\alpha,n) \right), \right.$$
$$\left. \times \left((\lambda_S - \lambda_{VS}) C_{co}(\alpha,n) + \chi^{\frac{2}{\alpha}} \lambda_{VS} C_{cr}(\alpha,n) \right) \right), \quad (39)$$

which resulting in the optimal vertically/horizontally polarized SN densities as $\hat{\lambda}_{VS} = \hat{\lambda}_{HS} = \frac{\lambda_S}{2}$.

D. DAS DESIGN STRATEGIES FOR POLARIZED DAS

From Corollary 1, by exploiting the dual-polarized DAS, the interference from the cross polarized DA ports can be lessened and the antenna selection diversity gain with $\bar{N}$ can be achieved. If the conventional co-polarized DAS is exploited, the antenna selection diversity gain with $2\bar{N}(= N)$ is achieved, but allowing more spatial interference compared to the dual-polarized DAS.

To compare their channel OPs analytically, we consider that vertically/horizontally polarized SN densities are given as $\lambda_{VS} = \lambda_{HS} = \lambda_S/2$. In the co-polarized DAS, each DA port has $2\bar{N}$ co-polarized antennas. Then, from Corollary 1, the channel OP of the dual-polarized DAS can be given as

$$P_{out,DP}(\chi, \bar{N}, \bar{\gamma}_{th})$$
$$\approx 1 - \sum_{n=1}^{\bar{N}} \frac{{}^{\bar{N}}C_n(-1)^{n+1}}{1 + \frac{\lambda_S}{2\pi \lambda_D} \left(1 + \chi^{\frac{4}{\alpha}} \right) C_{co}(\alpha,n)(n\bar{\gamma}_{th})^{\frac{2}{\alpha}}}. \quad (40)$$

By following a similar approach, the channel OP of the co-polarized DAS with $2\bar{N}$ antennas at each DA port can also be derived as

$$P_{out,CP}(2\bar{N}, \bar{\gamma}_{th}) = 1 - \sum_{n=1}^{2\bar{N}} \frac{{}^{2\bar{N}}C_n(-1)^{n+1}}{1 + \frac{\lambda_S}{\pi \lambda_D} C_{co}(\alpha,n)(n\bar{\gamma}_{th})^{\frac{2}{\alpha}}}. \quad (41)$$

Remark 3: We note that $P_{out,CP}(2\bar{N}, \bar{\gamma}_{th})$ in (41) can be rewritten as

$$P_{out,CP}(2\bar{N}, \bar{\gamma}_{th}) \approx 1 - \sum_{n=0}^{2\bar{N}-1} \Delta_n(\gamma_{th}), \quad (42)$$

where $\Delta_n(\gamma_{th}) = \Delta_{n-1}(\gamma_{th}) - (\delta_n - \delta_{n-1})$ with

$$\Delta_0(\gamma_{th}) = \frac{1}{1 + \frac{\lambda_S}{\pi \lambda_D} C_{co}(\alpha, 1)(\bar{\gamma}_{th})^{\frac{2}{\alpha}}}, \quad (43)$$

and $\delta_0 = \delta_{-1} = 0$. In addition,

$$\delta_n = \frac{1}{1 + \frac{\lambda_S}{\pi \lambda_D} C_{co}(\alpha, n)(n\bar{\gamma}_{th})^{\frac{2}{\alpha}}}$$
$$- \frac{1}{1 + \frac{\lambda_S}{\pi \lambda_D} C_{co}(\alpha, n+1)((n+1)\bar{\gamma}_{th})^{\frac{2}{\alpha}}}.$$

Accordingly, $\Delta_n(\gamma_{th}) > \Delta_{n+1}(\gamma_{th})$. Therefore, the rate of decrease in the channel OP slows down as the number of antennas increases. □

Remark 4: We note that (40) can be rewritten as

$$P_{out,DP}(\chi, \bar{N}, \bar{\gamma}_{th}) \approx 1 - \sum_{n=1}^{\bar{N}} \frac{{}^{\bar{N}}C_n(-1)^{n+1}}{1 + \frac{\lambda_S}{\pi \lambda_D} C_{co}(\alpha,n)(n\bar{\gamma}_{th}')^{\frac{2}{\alpha}}}, \quad (44)$$

where $\bar{\gamma}_{th}' = \bar{\gamma}_{th} \left(\frac{1 + \chi^{\frac{4}{\alpha}}}{2} \right)^{\frac{\alpha}{2}}$. By comparing (41) and (44), $P_{out,DP}(\chi, \bar{N}, \bar{\gamma}_{th})$ can be regarded as the channel OP of the single polarized DAS with $\bar{N}$ DA port antennas and the effective SINR threshold $\bar{\gamma}_{th}'$. Because $\frac{1 + \chi^{\frac{4}{\alpha}}}{2} \leq 1$, the polarization decreases the effective SINR threshold. From (42) and (43), a more decrease in the outage probability can be expected for a small χ. □

From Remark 3 and 4, when χ is small[3] or the number of transmit antennas is large, the dual-polarized DAS outperforms the conventional co-polarized DAS. Therefore, for a given number of transmit antennas, we find χ_{cross} such that the analytic channel OPs are the same for both dual-polarized DAS and co-polarized DAS. If $\chi > \chi_{cross}$, the dual-polarized DAS is deployed. Otherwise, co-polarized DAS is chosen for downlink DAS.

V. SIMULATION

Computer simulations have been performed to evaluate the performance of downlink polarized DAS. We consider the DA ports and SNs are distributed according to independent homogeneous PPP in the area of $10,000(100 \times 100)$ m^2. Specifically, the number of nodes are given as the product of node density and the deployment area (i.e., $10,000(100 \times 100)$ m^2 in our simulation) and the location of each node

---

[3]In [45] and [46] (and references therein), extensive measurements are conducted to model and analyze the radio propagation for the dual-polarized MIMO system and the XPD varies according to the conditions of the channel environment (i.e., LoS or NLos, the operating frequency, etc.).

TABLE 2. Simulation parameters for downlink polarized DAS.

Parameter	Value
Size of deployment area	$10,000(100 \times 100)$ m^2
Transmit power (P_{tx})	100 mW
Transmission bandwidth (BW)	$100 \, MHz$
Path-loss exponent (α)	2.8
Packet duration (T_p)	$20 \mu sec$
Packet size (N_b)	[125, 400] Bytes
Range of SINR threshold ($\bar{\gamma}_{th}$)	[0 : 0.22 : 2]
Noise power at each SN	316 µW
Inverse of XPD (χ)	[0 : 0.1 : 1]
Number of transmit antennas (N)	[2 : 2 : 20]
Densities of polarized SNs ($\lambda_{VS}, \lambda_{HS}$)	$\lambda_{VS} = \lambda_{HS} = 0.01$ nodes/m^2
Densities of polarized DA ports ($\lambda_{VD}, \lambda_{HD}$)	[0.2 : 0.2 : 0.8] nodes/m^2

is uniform random variable defined on the given area.[4] Throughout the simulations, the transmit power for each DA port is set as 100 mW and the noise power at each SN is 316 µW. The path-loss exponent is $\alpha = 2.8$. To see how the outage probabilities analyzed in (14) and (31) are relevant to the smart factory applications, we consider typical communication requirements for the IIoT [47], [48], where the transmission bandwidth (BW) is set as 100 MHz and the packet duration (T_p) is $20 \mu sec$. The detailed simulation parameters are summarized in Table 2. We note that, when the packet size (N_b) is varying as $N_b \in [125, 400]$ Bytes, the range of SINR threshold, $\bar{\gamma}_{th}$, from (18) is given as $0.414 \leq \bar{\gamma}_{th} \leq 2.03$ from (18). In addition, throughout the simulations, the SNs with a vertically (respectively, horizontally) polarized antenna are distributed according to independent homogeneous PPP with a density λ_{VS} (respectively, λ_{HS}).

1) SINGLE-POLARIZED DAS

In Fig. 3, the channel OPs for vertically polarized SNs are evaluated when the vertically (respectively, horizontally) polarized SNs are distributed with $\lambda_{VS} = \lambda_{HS} = 0.01$ nodes/m^2. In addition, DA ports with vertically (respectively, horizontally) polarized antennas are distributed with $\lambda_{VD} = \lambda_{HD} = 1.0$ nodes/m^2. From Fig. 3, as SINR threshold, $\bar{\gamma}_{th}$, increases, the channel OP also increases. Furthermore, from Fig. 3, as the number of transmit antennas increases, the channel OP decreases, which implies that the desired signal from the serving DA port to the reference SN can be more effectively transferred thanks to the antenna selection diversity.

---

[4]We note that the homogeneous PPP is defined on the unbounded two-dimensional space. Accordingly, when the size of deployment area is small, there may be difference between the analytic and simulation results. This is because the interference beyond the deployment area is not considered in the simulation results. Fortunately, the DA ports with a large distance from the origin (i.e., the location of the typical reference SN) cause small interference due to large path-loss. Therefore, as the size of deployment area becomes larger, the accuracy of the simulation results increases. It is also found that when the deployment area is set as $10,000(100 \times 100)$ m^2, the theoretical analysis tracks the simulation results quite closely.
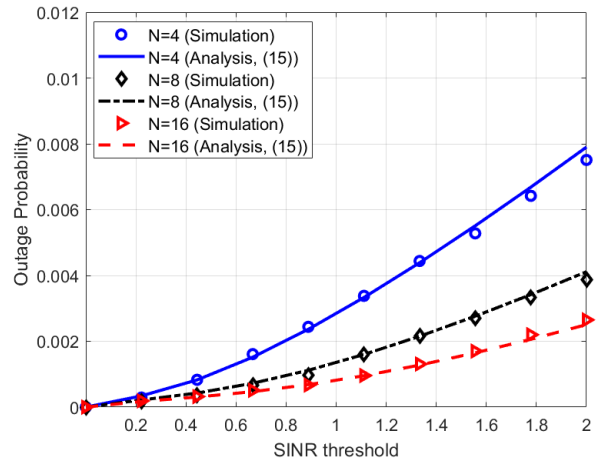

FIGURE 3. Channel OPs for various SINR threshold when $\lambda_D = 0.5$ nodes/m^2 and $N = \{4, 8, 16\}$.
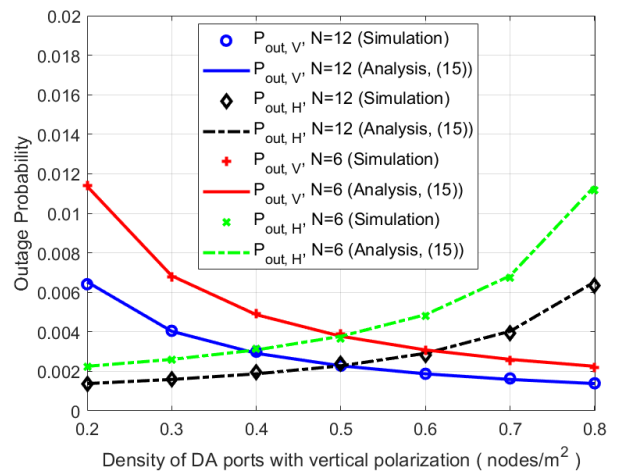

FIGURE 4. Channel OPs, $P_{out,V}$ and $P_{out,H}$ for various densities of vertically polarized DA ports (λ_{VD}) when $\lambda_{VD} + \lambda_{HD} = 1.0$ nodes/m^2, $\lambda_{VS} = \lambda_{HS} = 0.01$ nodes/m^2, and $N = \{6, 12\}$.

In Fig. 4, the channel OPs, $P_{out,V}$ and $P_{out,H}$ are evaluated for various densities of vertically polarized DA ports (λ_{VD}) when $\lambda_{VD} + \lambda_{HD} = 1.0$ nodes/m^2 and $\lambda_{VS} = \lambda_{HS} = 0.01$ nodes/m^2. Here, the SINR threshold, $\bar{\gamma}_{th}$, is set as $\bar{\gamma}_{th} = 1$ and the inverse of XPD is set as $\chi = 0.3$. The overall OP with $N = 12$ is smaller than that with $N = 6$. In addition, it can be found that the channel OP for SNs with p polarization decreases as λ_{pD} increases, which coincides with Lemma 1 and the discussion in Section III-B. Specifically, as λ_{pD} increases, C_p in (21) decreases, resulting in smaller channel OPs. Furthermore, we can also find that when $\lambda_{VD} = \lambda_{HD}$, $\max(P_{out,V}, P_{out,H})$ is minimized, which is also discussed in Section III-B.

In Fig. 5, the channel OPs for vertically polarized SNs are evaluated for various χ when the vertically (respectively, horizontally) polarized SNs are distributed with $\lambda_{VS} = \lambda_{HS} = 0.01$ nodes/m^2. In addition, DA ports with vertically (respectively, horizontally) polarized antennas are distributed with $\lambda_{VD} = \lambda_{HD} = 1.0$ nodes/m^2. The SINR threshold is set as $\bar{\gamma}_{th} = 1.0$. For comparison purposes, the channel
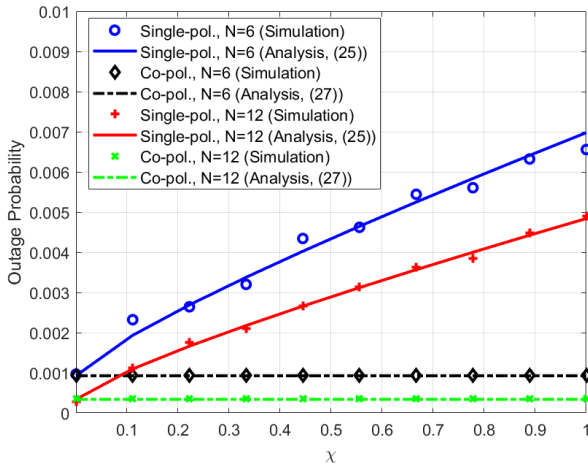
FIGURE 5. Channel OPs for various χ when $\lambda_D = \lambda_{VD} + \lambda_{HD} = 2.0$ nodes/m², $\lambda_S = \lambda_{VS} + \lambda_{HS} = 0.02$ nodes/m², and $N = \{6, 12\}$.
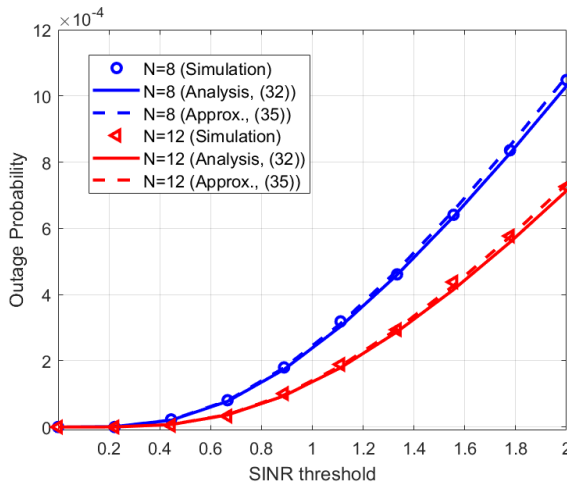

FIGURE 6. Channel OPs for dual-polarized DAS when $\lambda_D = 2.0$ nodes/m² and $N = \{8, 12\}$.

OPs for the conventional co-polarized DAS are also evaluated with $\lambda_S = 0.02$ nodes/m² and $\lambda_D = 2.0$ nodes/m². From the figure, as χ decreases, the channel OP decreases for the single-polarized DAS. That is, for a small χ, the interference from the cross polarized DA ports is effectively reduced. As discussed in Remark 2, the single-polarized DAS exhibits higher channel OP than the conventional co-polarized DAS and when $\chi = 0$, they have the same channel OP.

2) DUAL-POLARIZED DAS
In Fig. 6, the channel OPs are evaluated when the dual-polarized DAS is deployed with $\lambda_D = 2.0$ nodes/m² and $N = \{8, 12\}$. Again, from Fig. 6, as the number of transmit antennas increases, the channel OP decreases. In addition, the approximation in (34) coincides with the simulation results and accordingly, the interference in the dual-polarized DAS can be approximated as that from a homogeneous PPP with copolarized DAS and an effective node density ($\lambda_{VS} + \chi^{\frac{4}{\alpha}} \lambda_{HS}$) as discussed in Corollary 1.
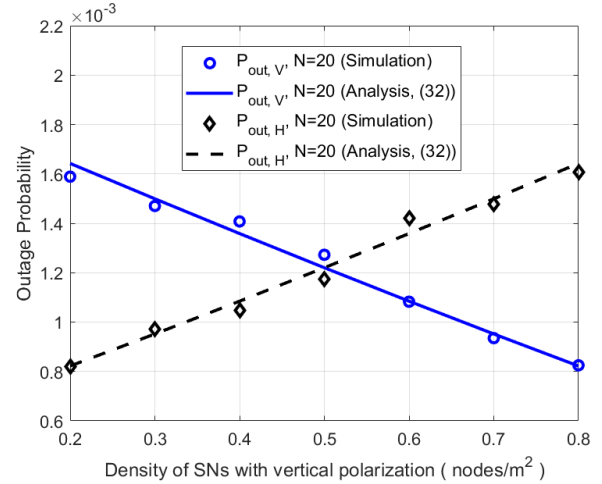

FIGURE 7. Channel OPs, $P_{out,V}$ and $P_{out,H}$ for various densities of vertically polarized SNs (λ_{VS}) when $\lambda_{VS} + \lambda_{HS} = 0.02$ nodes/m², $\lambda_D = 1.0$ nodes/m², and $N = 20$.

In Fig. 7, the channel OPs, $P_{out,V}$ and $P_{out,H}$ are evaluated for various densities of vertically polarized SNs (λ_{VS}) with $N = 20$ when $\lambda_{VS} + \lambda_{HS} = 0.02$ nodes/m² and $\lambda_D = 1.0$ nodes/m². Here, the SINR threshold, $\bar{\gamma}_{th}$, is set as $\bar{\gamma}_{th} = 1$ and the inverse of XPD is set as $\chi = 0.3$. It can be found that the channel OP for SNs with p polarization increases as λ_{pS} increases, as discussed in Section IV-C. That is, as λ_{pS} increases, the active DA ports to support the co-polarized SNs increases and they cause interference to the reference co-polarized SN. Therefore, when $\lambda_{VS} = \lambda_{HS} = \frac{\lambda_S}{2}$, $\max(P_{out,V}, P_{out,H})$ is minimized, which is also discussed in Section IV-C.

In Fig. 8, we compare the channel OPs for the dual-polarized DAS and the conventional co-polarized DAS with the same node densities. Specifically, we set $\lambda_{VS} = \lambda_{HS} = 0.01$ nodes/m² and $\lambda_D = 2.0$ nodes/m² for the dual-polarized DAS and $\lambda_S = 0.02$ nodes/m² and $\lambda_D = 2.0$ nodes/m² for the conventional DAS. In Fig. 8 (a), the OPs are evaluated for various χ with $N = 16$. As χ increases, the channel OP of the dual-polarized DAS increases. That is, large χ induces strong interference from the cross-polarized DA ports. In contrast, the conventional co-polarized DAS is not affected by χ. From the figure, when χ is small (specifically, $\chi < \chi_{cross} = 0.451$), the dual-polarized DAS outperforms the co-polarized DAS. In Fig. 8 (b), the OPs are evaluated for various numbers of transmit antennas with $\chi = 0.15$. As the number of transmit antennas increases, the overall channel OPs decrease for both dual-polarized DAS and co-polarized DAS. Interestingly, for $N > 5$, the dual-polarized DAS outperforms the co-polarized DAS because the rate of decrease in the channel OP slows down as the number of antennas increases as discussed in Remark 3. Accordingly, from Fig. 8 (a) and (b), when χ is small or the number of transmit antennas become large, the dual-polarized DAS outperforms the conventional co-polarized DAS, which coincides with Remark 3 and 4. Therefore, based on the network parameters such as the number of transmit antennas

TABLE 3. Preferable DAS structure yielding lower channel OPs.

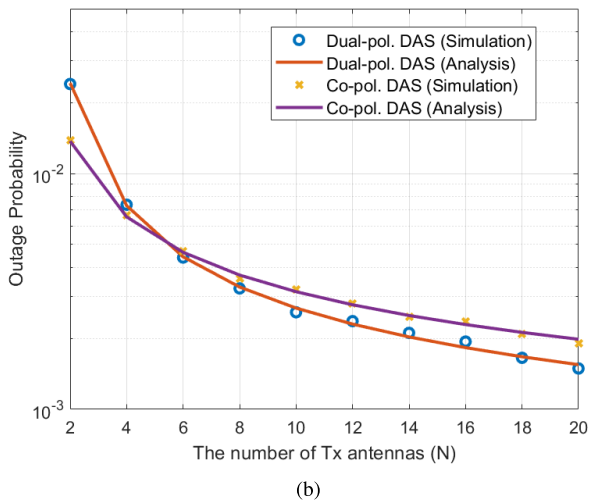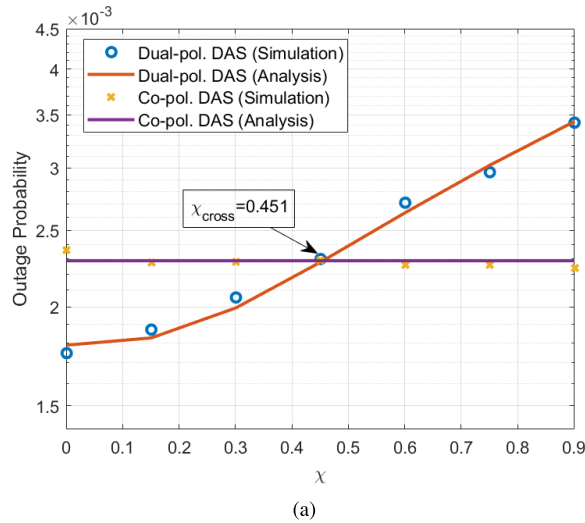|		The number of transmit antennas (N)	
		Small	Large
χ	Small	Co/Dual-polarized DAS	Dual-polarized DAS
	Large	Co-polarized DAS	Co/Dual-polarized DAS

(a)

(b)

FIGURE 8. Channel OPs of the dual-polarized DAS and the conventional co-polarized DAS for (a) various χ with $N = 16$ and (b) various numbers of transmit antennas (N) with $\chi = 0.15$ when $\lambda_S = 0.02$ nodes/m^2 and $\lambda_D = 2.0$ nodes/m^2.

and χ, it can be chosen which DAS structure is suitable to minimize the channel OPs. In Table 3, the preferable DAS structure yielding lower channel OPs is summarized based on the analytic results.

VI. CONCLUSION

In this paper, we have investigated the channel OP in the polarized DAS, where SNs and DA ports are randomly distributed according to independent PPP and either vertically or horizontally polarized antennas are deployed at both SNs and DA ports. By using the stochastic geometry, we derive the channel OP of the single-polarized DAS in a closed form and show how we can optimize the network parameters

to minimize the channel OP. Furthermore, by investigating the effects of node density and polarization on the channel OP, we develop the dual-polarized DAS, in which the DA port density is maintained compared to the conventional co-polarized DAS, while the interference can be lessened through the polarization selection. From the performance analysis for the dual-polarized DAS, when χ is small or the number of transmit antennas become large, the dual-polarized DAS outperforms the conventional co-polarized DAS, which is also confirmed through computer simulations and gives us a useful insight into the design of the polarized DAS to minimize the channel OPs.

REFERENCES

[1] E. Sisinni, A. Saifullah, S. Han, U. Jennehag, and M. Gidlund, "Industrial Internet of Things: Challenges, opportunities, and directions," *IEEE Trans. Ind. Informat.*, vol. 14, no. 11, pp. 4724–4734, Nov. 2018.

[2] A. Mahmood, L. Beltramelli, S. Fakhrul Abedin, S. Zeb, N. I. Mowla, S. A. Hassan, E. Sisinni, and M. Gidlund, "Industrial IoT in 5G-and-Beyond networks: Vision, architecture, and design trends," *IEEE Trans. Ind. Informat.*, vol. 18, no. 6, pp. 4122–4137, Jun. 2022.

[3] X. Pan and Z. Zheng, "Cooperative distributed antenna systems based secure communications for industrial Internet of Things," in *Proc. IEEE 20th Int. Conf. Commun. Technol. (ICCT)*, Oct. 2020, pp. 790–794.

[4] S. Shen, J. Kim, C. Song, and B. Clerckx, "Wireless power transfer with distributed antennas: System design, prototype, and experiments," *IEEE Trans. Ind. Electron.*, vol. 68, no. 11, pp. 10868–10878, Nov. 2021.

[5] T. Onishi, E. Takahashi, Y. Nishikawa, and S. Maruyama, "AppDAS: An application QoS-aware distributed antenna selection for 5G industrial applications," in *Proc. IEEE 20th Consum. Commun. Netw. Conf.*, Jan. 2023, pp. 1027–1032.

[6] S. Jeong, O. Simeone, A. Haimovich, and J. Kang, "Beamforming design for joint localization and data transmission in distributed antenna systems," in *Proc. IEEE Global Conf. Signal Inf. Process.*, Dec. 2013, pp. 879–882.

[7] H. Kim, E. Park, H. Park, and I. Lee, "Beamforming and power allocation designs for energy efficiency maximization in MISO distributed antenna systems," *IEEE Commun. Lett.*, vol. 17, no. 11, pp. 2100–2103, Nov. 2013.

[8] H. Siljak, K. Psara, and A. Philippou, "Distributed antenna selection for massive MIMO using reversing Petri nets," *IEEE Wireless Commun. Lett.*, vol. 8, no. 5, pp. 1427–1430, Oct. 2019.

[9] Z. Wei and C. Masouros, "Device-centric distributed antenna transmission: Secure precoding and antenna selection with interference exploitation," *IEEE Internet Things J.*, vol. 7, no. 3, pp. 2293–2308, Mar. 2020.

[10] J. Park and B. Clerckx, "Multi-user linear precoding for multi-polarized massive MIMO system under imperfect CSIT," *IEEE Trans. Wireless Commun.*, vol. 14, no. 5, pp. 2532–2547, May 2015.

[11] S. Stern and R. F. H. Fischer, "Quaternion-valued multi-user MIMO transmission via dual-polarized antennas and QLLL reduction," in *Proc. 25th Int. Conf. Telecommun. (ICT)*, Jun. 2018, pp. 63–69.

[12] P. Nagaradjane and T. Muthu, "Joint transmitter-receiver design for the uplink multi-user-MIMO transmission aided by polarization multiplexing," in *Proc. Int. Conf. Commun. Signal Process. (ICCSP)*, Apr. 2015, pp. 1946–1950.

[13] P. Palanisamy and M. Subramani, "An integrated antenna for cognitive radio wireless sensor networks and HD video transmission applications," *Int. J. RF Microw. Comput.-Aided Eng.*, vol. 31, no. 11, pp. 1–15, Nov. 2021.

[14] X.-Q. Zhu, Y.-X. Guo, and W. Wu, "Miniaturized dual-band and dual-polarized antenna for MBAN applications," *IEEE Trans. Antennas Propag.*, vol. 64, no. 7, pp. 2805–2814, Jul. 2016.

[15] Y.-M. Zhang and J.-L. Li, "A dual-polarized antenna array with enhanced interport isolation for far-field wireless data and power transfer," *IEEE Trans. Veh. Technol.*, vol. 67, no. 11, pp. 10258–10267, Nov. 2018.

[16] H. Jin, K. Liu, M. Zhang, L. Zhang, G. Lee, E. N. Farag, D. Zhu, E. Onggosanusi, M. Shafi, and H. Tataria, "Massive MIMO evolution toward 3GPP release 18," *IEEE J. Sel. Areas Commun.*, vol. 41, no. 6, pp. 1635–1654, Jun. 2023.

[17] T. Oh, Y.-G. Lim, C.-B. Chae, and Y. Lee, "Dual-polarization slot antenna with high cross-polarization discrimination for indoor small-cell MIMO systems," *IEEE Antennas Wireless Propag. Lett.*, vol. 14, pp. 374–377, 2015.

[18] A.-N. Nguyen, V. Hoang Le, N. Nguyen-Trong, M. Radfar, A. Ebrahimi, K. Phan, and A. Desai, "Dual-polarized slot antenna for full-duplex systems with high isolation," *IEEE Trans. Antennas Propag.*, vol. 69, no. 11, pp. 7119–7124, Nov. 2021.

[19] B. Cai, C. Yue, J. Li, and P. Zhu, "Downlink spectral efficiency of multi-user distributed antenna systems under a stochastic geometry model," in *Proc. 9th Int. Conf. Wireless Commun. Signal Process. (WCSP)*, Oct. 2017, pp. 1–6.

[20] Y. Lin and W. Yu, "Downlink spectral efficiency of distributed antenna systems under a stochastic model," *IEEE Trans. Wireless Commun.*, vol. 13, no. 12, pp. 6891–6902, Dec. 2014.

[21] H. ElSawy, A. Sultan-Salem, M.-S. Alouini, and M. Z. Win, "Modeling and analysis of cellular networks using stochastic geometry: A tutorial," *IEEE Commun. Surveys Tuts.*, vol. 19, no. 1, pp. 167–203, 1st Quart., 2017.

[22] J. G. Andrews, A. K. Gupta, and H. S. Dhillon, "A primer on cellular network analysis using stochastic geometry," 2016, *arXiv:1604.03183*.

[23] J. G. Andrews, F. Baccelli, and R. K. Ganti, "A tractable approach to coverage and rate in cellular networks," *IEEE Trans. Commun.*, vol. 59, no. 11, pp. 3122–3134, Nov. 2011.

[24] H. S. Dhillon, R. K. Ganti, F. Baccelli, and J. G. Andrews, "Modeling and analysis of K-Tier downlink heterogeneous cellular networks," *IEEE J. Sel. Areas Commun.*, vol. 30, no. 3, pp. 550–560, Apr. 2012.

[25] M. Haenggi, J. G. Andrews, F. Baccelli, O. Dousse, and M. Franceschetti, "Stochastic geometry and random graphs for the analysis and design of wireless networks," *IEEE J. Sel. Areas Commun.*, vol. 27, no. 7, pp. 1029–1046, Sep. 2009.

[26] M. Haenggi, *Stochastic Geometry for Wireless Networks*. Cambridge, U.K.: Cambridge Univ. Press, 2012.

[27] C.-H. Lee and M. Haenggi, "Interference and outage in Poisson cognitive networks," *IEEE Trans. Wireless Commun.*, vol. 11, no. 4, pp. 1392–1401, Apr. 2012.

[28] X. Liu and M. Haenggi, "Toward quasiregular sensor networks: Topology control algorithms for improved energy efficiency," *IEEE Trans. Parallel Distrib. Syst.*, vol. 17, no. 9, pp. 975–986, Sep. 2006.

[29] A. Imani, M. Eslami, and J. Hazhizhar, "Stochastic geometry based analysis of coverage in wireless sensor networks," in *Proc. Electr. Eng. (ICEE), Iranian Conf.*, May 2018, pp. 698–703.

[30] Y. Deng, L. Wang, M. Elkashlan, A. Nallanathan, and R. K. Mallik, "Physical layer security in three-tier wireless sensor networks: A stochastic geometry approach," *IEEE Trans. Inf. Forensics Security*, vol. 11, no. 6, pp. 1128–1138, Jun. 2016.

[31] A. M. Hunter, J. G. Andrews, and S. Weber, "Transmission capacity of ad hoc networks with spatial diversity," *IEEE Trans. Wireless Commun.*, vol. 7, no. 12, pp. 5058–5071, Dec. 2008.

[32] M. U. Sheikh, K. Ruttik, R. Jäntti, and J. Hämäläinen, "Distributed antenna system in 3GPP specified industrial environment," in *Proc. IEEE 93rd Veh. Technol. Conf. (VTC-Spring)*, Apr. 2021, pp. 1–6.

[33] Y. Hu, B. L. Ng, Y.-H. Nam, J. Yuan, G. Xu, and J.-Y. Seol, "Distributed FD-MIMO: Cellular evolution for 5G and beyond," 2017, *arXiv:1704.00647*.

[34] O. Haliloglu, H. Yu, C. Madapatha, H. Guo, F. E. Kadan, A. Wolfgang, R. Puerta, P. Frenger, and T. Svensson, "Distributed MIMO systems for 6G," in *Proc. Joint Eur. Conf. Netw. Commun. 6G Summit*, Jun. 2023, pp. 156–161.

[35] A. Molisch and M. Win, "Mimo systems with antenna selection," *IEEE Microwave Mag.*, vol. 5, no. 1, pp. 46–56, 2004.

[36] Z. Liu and S. Feng, "Antenna selection for full-duplex distributed antenna systems," *IEEE Access*, vol. 7, pp. 132516–132524, 2019.

[37] S. M. Yu and S.-L. Kim, "Downlink capacity and base station density in cellular networks," in *Proc. 11th Int. Symp. Workshops Model. Optim. Mobile, Ad Hoc Wireless Netw. (WiOpt)*, May 2013, pp. 119–124.

[38] D. Stoyan, W. Kendall, and J. Mecke, *Stochastic Geometry and its Applications*. Hoboken, NJ, USA: Wiley, 1996.

[39] H. A. David and H. N. Nagaraja, *Order Statistics*. Hoboken, NJ, USA: Wiley, 2004.

[40] J. Park, J.-P. Hong, W. Shin, and S. Kim, "Performance analysis of distributed antenna system for downlink ultrareliable low-latency communications," *IEEE Syst. J.*, vol. 15, no. 1, pp. 518–525, Mar. 2021.

[41] H.-R. Chuang and L.-C. Kuo, "3-D FDTD design analysis of a 2.4-GHz polarization-diversity printed dipole antenna with integrated balun and polarization-switching circuit for WLAN and wireless communication applications," *IEEE Trans. Microwave Theory Techn.*, vol. 51, no. 2, pp. 374–381, Feb. 2003.

[42] S. Sanayei and A. Nosratinia, "Antenna selection in MIMO systems," *IEEE Commun. Mag.*, vol. 42, no. 10, pp. 68–73, 2004.

[43] B. S. Tan, K. H. Li, and K. C. Teh, "Transmit antenna selection systems: A performance comparison of different types of receiver schemes," *IEEE Veh. Technol. Mag.*, vol. 8, no. 3, pp. 104–112, Sep. 2013.

[44] E. W. Weisstein. (2003). *Incomplete Beta Function*. [Online]. Available: https://mathworld.wolfram.com/

[45] M. B. Khalilsarai, T. Yang, S. Haghighatshoar, X. Yi, and G. Caire, "Dual-polarized FDD massive MIMO: A comprehensive framework," *IEEE Trans. Wireless Commun.*, vol. 21, no. 2, pp. 840–854, Feb. 2022.

[46] C. Guo, F. Liu, S. Chen, C. Feng, and Z. Zeng, "Advances on exploiting polarization in wireless communications: Channels, technologies, and applications," *IEEE Commun. Surveys Tuts.*, vol. 19, no. 1, pp. 125–166, 1st Quart., 2017.

[47] M. Khoshnevisan, V. Joseph, P. Gupta, F. Meshkati, R. Prakash, and P. Tinnakornsrisuphap, "5G industrial networks with CoMP for URLLC and time sensitive network architecture," *IEEE J. Sel. Areas Commun.*, vol. 37, no. 4, pp. 947–959, Apr. 2019.

[48] J.-P. Hong, J. Park, W. Shin, and S. Baek, "Spectral efficient resource allocation for URLLC in distributed antenna systems," *IEEE Trans. Veh. Technol.*, vol. 69, no. 12, pp. 15057–15067, Dec. 2020.

JUNGSUN UM received the B.S. and M.S. degrees in electronic and electrical engineering from Sungkyunkwan University, Suwon, Republic of Korea, in 2004 and 2006, respectively, and the Ph.D. degree in electrical engineering from Korea Advanced Institute of Science and Technology, Daejeon, Republic of Korea, in 2017. Since 2006, he has been with the Electronics and Telecommunications Research Institute, Daejeon, where he is currently a Principal Member. His main research interests include spectrum-sharing technologies, interference analysis, wireless communication systems, and signal processing for digital television.

JAEHYUN PARK (Member, IEEE) received the B.S. and Ph.D. (M.S. and Ph.D. joint program) degrees in electrical engineering from Korea Advanced Institute of Science and Technology (KAIST), in 2003 and 2010, respectively. From 2010 to 2013, he was a Senior Researcher with the Electronics and Telecommunications Research Institute (ETRI), where he worked on transceiver design and spectrum sensing for cognitive radio systems. From 2013 to 2014, he was a Postdoctoral Research Associate with the Electrical and Electronic Engineering Department, Imperial College London. He is currently a Professor with the Electronic Engineering Department, Pukyong National University, South Korea. His research interests include signal processing for wireless communications and radar systems, with a focus on detection and estimation for MIMO systems, MIMO radar, cognitive radio networks, and joint information and energy transfer.

● ● ●